2023 IEEE/ASME International Conference on Advanced Intelligent Mechatronics (AIM)
June 28-30, 2023. Seattle, Washington, USA

Torque model and drive method for developing closed-loop orientation control of spherical brushless direct current motor

Sangheon Lee, and Hungsun Son*

Abstract— **This paper presents a novel multi-degree of freedom actuator driven by three-phase inputs, referred to here as a spherical brushless direct current motor (SBLDC), and its closed-loop control system. The SBLDC can simultaneously generate both spinning and tilting torque for the orientation control of a rotating rotor using two independent BLDC drivers commercially available. The mathematical torque model is derived by three-phase inputs and rotor orientation. A drive method is developed based on the torque model to achieve desired three-dimensional torque. The closed-loop orientation control system based on cascade PID control is designed to validate the torque model and drive method. Finally, the performance of the SBLDC is demonstrated through the numerical simulation, which shows the compact three-phase spherical actuator's potential for precise three-dimensional orientation control.**

I. Introduction

Actuators and manipulators with multi-degree of freedom (DOF) motion are widely used in mechatronics systems that require highly precise and dexterous multi-DOF motion control. The spherical wheel motor (SWM) [1] has been developed over several decades to meet this demand for robotics and mobility systems. With the ability to spin and tilt an output shaft with a single actuator, it simplifies system configuration and reduces the number of required actuators. For instance, a 3-DOF rotational stage was developed for 6-DOF conformal printing of curved electronics [2], and a robotic wrist can be one of its possible applications because the SWM can avoid singularity in manipulation [3].

The SWM is composed of multiple layers of stator electromagnets (EMs) and rotor permanent magnets (PMs). SWM controllers compute the current inputs of all the EMs, to generate the required three-dimensional torque corresponding to the rotor's orientation. However, real-time control is challenging due to the nonlinearity of the torque and magnetic field, which depend on the current inputs and rotor orientation. Open-loop control (OL) was developed in [4], providing an inverse torque model for real-time control of the tilting torque. It serves as the basis for developing a closed-loop control (CL) structure, which overcomes OL control limitations, such as undesired transient responses and tracking accuracy due to disturbances and uncertainties.

In [5], an OL system with an input-shaping technique and a CL system consisting of a PD control and a high-gain observer were proposed. The input-shaping techniques improved transient response and reduced oscillation of the OL system but still showed poorer performance than the CL system. However, the CL system had limitations as it depends on the orientation measurement system, requiring high computational loads to transform magnetic field measurements into orientation due to nonlinearity [6]. To overcome this limitation, a direct field-feedback control was proposed to control rotor orientation by directly feeding back magnetic field measurements without the transformation process [7]. However, CL systems based on magnetic field measurements require a number of linear Hall-effect sensors and a calibration process. For practical applications, the CL system was developed using the inertial measurement unit (IMU) instead of Hall-effect sensors, reducing the number of sensors and allowing for more intuitive orientation control [8]. Additionally, the CL system in [8] shows great robustness in the presence of system uncertainty and external disturbance thanks to the proposed H_2-H_∞ control.

Significant progress has been made in the development and control of the SWM, bringing it closer to practical implementation. However, most control systems for the SWM rely on the inverse torque model, which necessitates heavy computation due to redundant current inputs, typically higher than the controllable DOF. These redundant inputs also require high-cost drivers and increase system complexity due to numerous independent EMs.

To overcome these limitations, a three-phase type spherical motor called a tiered-type permanent magnet spherical motor (T-PMSPM) has been developed [9]. The T-PMSPM design simplifies the field and torque model compared to the SWM in several ways. First, the polarity of the rotor field only changes along the azimuthal direction while the polarity of the SWM's rotor field changes along both the polar and azimuthal direction. This allows for a simpler expression of the rotor field in terms of rotor orientation. Second, the EM layers of the stator are separated into tilting and spinning layers, while the SWM lacks this separation. Consequently, T-PMSPM can independently control the torque for tilting and spinning motion. Additionally, both tilting and spinning layers are driven by three-phase current inputs, so the number of current inputs cannot exceed six, regardless of the number of EMs. In contrast, the SWM controls all EMs independently, making the torque model more complex as the number of EMs increases.

This work was supported in part by the National Research Foundation of Korea (NRF) grant funded by the Korea government (MSIT) (No. 2020R1A6A1A03040570), the Ministry of Trade, Industry and Energy (MOTIE) and Korea Evaluation Institute of Industrial Technology (KEIT) through the Helicopter Electric Multiple Tail Rotor Technology R&D program under Grant (RS-2022-00155776), and, Future Innovation Research Funds of the Ulsan National Institute of Science and Technology (1.230014.01), respectively.

The authors are with the department of Mechanical Engineering, Ulsan National Institute of Science and Technology, Ulsan 44919, South Korea. (e-mail: ssle8653@unist.ac.kr; hson@unist.ac.kr).
* Corresponding author: *Hungsun Son*

978-1-6654-7633-1/23/$31.00 ©2023 IEEE

However, to the best of our knowledge, torque drive and orientation control systems have not been developed for the T-PMSPM. Research has primarily focused on torque characteristics [9]-[11], magnetic field analysis [12], and orientation measurement systems [13]. Furthermore, the T-PMSPM is designed based on the principle of the permanent magnet synchronous motor (PMSM), which may necessitate field-oriented control, increasing driver costs due to power electronics for current control.

To address these issues, this paper presents a spherical brushless direct current motor (SBLDC), a three-phase spherical motor designed based on the principle of the brushless direct current motor (BLDC). As a result, the SBLDC can be driven by conventional BLDC drivers, generating the torque through voltage control, making it simpler and more cost-effective than the PMSM driver. In addition, the torque drive method has been proposed to facilitate the development of a 3D orientation control system. The remainder of this paper offers the following.

1) A mechanical design of the SBLDC is presented, and operating torque model is proposed based on the dominant magnetic field of the rotor and the stator. In addition, the rotor dynamics are derived with the operating torque to validate the proposed CL system.
2) A torque drive method is proposed to generate the desired 3D torque magnitude and direction based on a six-step commutation of BLDC drivers. In addition, the CL system has been designed with orientation, angular rate control, and the torque drive method.
3) The performance of the SBLDC and its CL system is evaluated through numerical simulations using an air-core 6N8P SBLDC. The results confirm the effectiveness of the torque drive and orientation control, providing the basis for developing a robust and precise orientation control for practical applications such as robotic joints and gimbal systems.

II. Design and Dynamic Model of Spherical Brushless Direct Current Motor

The SBLDC in Fig. 1 illustrates a spherical rotor and stator configuration. The rotor consists of two spherical back-irons, on which p pairs of arc-shaped permanent magnets (PMs) are mounted to create a uniform magnetic field at the airgap. An IMU is affixed to the rotor and linked to the drivers via a slip ring, enabling continuous orientation measurement during rotation. The stator in Fig. 1(b) comprises three layers of electromagnets (EMs). Each layer includes Q slots with 3-phase BLDC windings. A middle layer, referred to as the spinning layer, is wound to produce the spinning torque, while the remaining two layers, referred to as the tilting layers, are responsible for generating the unbalanced magnetic force (UMF). The EMs of these tilting layers are wound in opposite directions, thereby effectively canceling out the UMF, leaving only the tilting torque intact. The spinning and tilting layers are driven independently by two separate BLDC drivers to generate the desired three-dimensional torque. As a result, the rotor can rotate in three-DOF via spherical plane bearing.

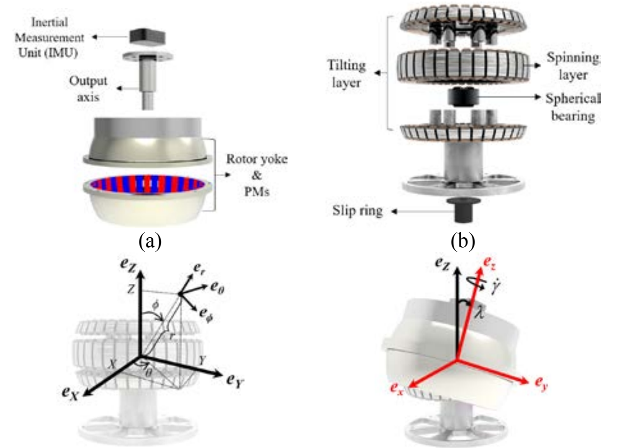

Fig.1 Spherical brushless direct current motor (a) Rotor. (b) Stator. (c) Assembly and coordinate system.

The pairs of PMs generate the magnetic field at the airgap $r = r_g$, expressed as $\mathbf{B} = B_r\mathbf{e}_r + B_\phi\mathbf{e}_\phi + B_\theta\mathbf{e}_\theta$ in the spherical coordinate $\{\mathbf{e}_r\ \mathbf{e}_\phi\ \mathbf{e}_\theta\}$. The polarity of the PM changes along the azimuthal direction, meaning that each component of the rotor field can be simplified into its fundamental harmonic, represented by the trigonometric function of θ as

$$B_i = B_{Ri}(\lambda,\phi)c_{p_R\theta-\delta_R}\ \ (i=r,\phi),\ B_\theta = B_{R\theta}(\lambda,\phi)s_{p_R\theta-\delta_R} \quad (1)$$

where the harmonic order of the rotor field p_R is equal to the number of the pole-pairs p. δ_R represents the phase shifts as the rotor spins and can be approximated as the electrical spinning angle $p\gamma$. The amplitudes of the dominant harmonics are dependent on the tilting angle of the rotor λ and the polar angle of the observation point ϕ.

The spinning layer is wound using a QN2pP BLDC winding layout to generate the spinning torque. It contains a working harmonic (WH) of order p_S equal to p_R. Thus, the magnetic field can be expressed by the dominant harmonic as

$$B_i = B_{Si}(\phi)s_{p_S\theta-\delta_S}\ \ (i=r,\phi),\ B_\theta = B_{S\theta}(\phi)c_{p_S\theta-\delta_S} \quad (2)$$

where δ_S is the phase of the spinning layer field and the amplitude of its harmonic is a function of ϕ. On the other hand, the tilting layer should contain a WH of order p_T equal to $p_R \pm 1$, in order to produce the UMF, not the spinning torque [15]. Therefore, QN2($p \pm 1$)P BLDC winding layout can be applied for the tilting layers. In this work, only $p_T = p_R+1$ is considered, and the tilting layer field can be expressed as

$$B_i = B_{Ti}(\phi)c_{p_T\theta-\delta_T}\ \ (i=r,\phi),\ B_\theta = B_{T\theta}(\phi)s_{p_T\theta-\delta_T} \quad (3)$$

where δ_T is the phase of the tilting layer field.

An input torque $\mathbf{T} = T_X\mathbf{e_X} + T_Y\mathbf{e_Y} + T_Z\mathbf{e_Z}$ acting on the rotor is generated by the interaction between the rotor and stator fields, where $\{\mathbf{e_X}, \mathbf{e_Y}, \mathbf{e_Z}\}$ is the stator fixed frame. It is sum of the spinning torque $\mathbf{T}_S$ and tilting torque $\mathbf{T}_T$. The rotor dynamics according to the input torque can be described using Lagrangian mechanics as

$$\mathbf{W}^T\mathbf{IW}\ddot{\boldsymbol{\eta}} = (\mathbf{RW})^T\mathbf{T} + \mathbf{T_C}(\boldsymbol{\eta},\dot{\boldsymbol{\eta}}) + \mathbf{T_D}(\boldsymbol{\eta},\dot{\boldsymbol{\eta}}) + \mathbf{T_G}(\boldsymbol{\eta}) \quad (4)$$

$$\boldsymbol{\omega} = \mathbf{W}\dot{\boldsymbol{\eta}} \quad (5)$$

where $\mathbf{R}$ is a rotational matrix expressed in terms of the XYZ Euler angles $\boldsymbol{\eta} = [\alpha\ \beta\ \gamma]^T$, and $\boldsymbol{\omega}$ is body angular rate in the rotor fixed frame{$\mathbf{e}_x$, $\mathbf{e}_y$, $\mathbf{e}_z$}; $\mathbf{I}$ is the moment of inertia tensor; $\mathbf{T}_C$ is the Coriolis-centrifugal torque; $\mathbf{T}_D$ is the frictional torque; $\mathbf{T}_G$ is the is the gravitational torque.

III. Torque Model and Drive

A. Torque model

The spinning torque in (6) can be expressed in terms of the dominant harmonics of the rotor field and spinning layer field based on the Maxwell stress tensor (MST).

$$\mathbf{T}_S = T_Z \mathbf{e}_\mathbf{Z} = T_S c_{\delta_{S\Delta}} \mathbf{e}_\mathbf{Z} \tag{6}$$

$$T_S(\lambda) = -\pi r_g^{\ 3} \mu_0^{-1} \int_0^\pi s_\phi^2 \left(B_{Rr} B_{S\theta} + B_{Sr} B_{R\theta} \right) d\phi \tag{7}$$

where the phase difference between the spinning layer and the rotor field $\delta_{S\Delta} = \delta_S - \delta_R$. T_S is function of λ which influences the rotor field B_{Rr} and $B_{R\theta}$. The detailed derivation can be found in Appendix A.

Similarly, tilting torque $\mathbf{T}_T$ can be derived based on the MST as

$$\mathbf{T}_T = T_X \mathbf{e}_\mathbf{X} + T_Y \mathbf{e}_\mathbf{Y} = -T_T s_{\delta_{T\Delta}} \mathbf{e}_\mathbf{X} + T_T c_{\delta_{T\Delta}} \mathbf{e}_\mathbf{Y} \tag{8}$$

$$T_T(\lambda) = -\frac{\pi r_g^{\ 3}}{2\mu_0} \int_0^\pi \left(B_{Rr} B_{T\phi} + B_{Tr} B_{R\phi} \right) s_\phi - \frac{B_{Rr} B_{T\theta} - B_{Tr} B_{R\theta}}{2} s_{2\phi} d\phi \tag{9}$$

where the phase difference between the tilting layer and the rotor field $\delta_{T\Delta} = \delta_T - \delta_R$.

B. Torque drive

The torque magnitude and direction are controlled by two BLDC drivers, one for the spinning layer and the other for the tilting layer, which are connected in a parallel configuration. The magnitude of the spinning torque can be controlled by manipulating the duty cycles of the spinning driver, $0 < d_S < 1$, as the spinning layer field can be assumed to be proportional to d_S. Thus, $\mathbf{T}_S$ can be modeled as

$$\mathbf{T}_S = \alpha_S d_S c_{\delta_{S\Delta}} \mathbf{e}_Z \tag{10}$$

where a spinning torque factor α_S is the function of λ as

$$\alpha_S(\lambda) = T_S(\lambda)\big|_{d_S=1} \tag{11}$$

Similarly, $\mathbf{T}_T$ can be modeled with the duty cycles of the tilting driver, $0 < d_T < 1$, and the tilting torque factor α_T as

$$\mathbf{T}_T = \alpha_T d_T \left(-s_{\delta_{T\Delta}} \mathbf{e}_\mathbf{X} + c_{\delta_{T\Delta}} \mathbf{e}_\mathbf{Y} \right) \tag{12}$$

$$\alpha_T(\lambda) = T_T(\lambda)\big|_{d_T=1} \tag{13}$$

The torque direction can be changed by manipulating the phase difference $\delta_{S\Delta}$ and $\delta_{T\Delta}$. Therefore, it is important to control the stator field phase according to δ_R. This can be done by selecting the appropriate combination of energizing the 3-phase stator poles, as detailed in Table I. The phases are described mathematically as

$$\delta_j = 3^{-1}\pi \left(k_j - 1 \right) \quad (j = S, T) \tag{14}$$

where k_S is the index for the spinning layer's switching, and k_T is the index for the tilting layers. Thus, there are six candidates for each spinning and tilting torque.

For obtaining the maximum spinning torque, selecting the appropriate phase difference, $\delta_{S\Delta}$, is important among the six candidates. The optimal candidate is determined based on the desired direction of the spinning torque $\mathbf{e}_{Sd}$. For positive T_s, if the desired direction is counterclockwise, the candidate closest to 0 is the optimal choice. If the desired direction is clockwise, the candidate closest to π is the best option. The optimal candidates also can be changed according to the rotor spinning angle because it affects the phase of the rotor field. Therefore, k_S can be determined according to $\mathbf{e}_{Sd}$ and δ_R.

The rotor spinning angle affects not only choosing the switching index but the magnitude by impacting cos($\delta_{S\Delta}$) in (6). To regulate the magnitude, d_S can be modified as

$$d_S = d_{Sd} / c_{\delta_{S\Delta}} \tag{15}$$

where d_{Sd} is a desired spinning duty cycle.

The tilting torque drive operates in two dimensions, allowing for six different torque candidates by changing the switching index. When the direction of the desired torque $\mathbf{e}_{Td}$ aligns with of the candidate torque vectors, the corresponding index can be selected. However, if $\mathbf{e}_{Td}$ does not match with any candidates, two candidates, $\mathbf{e}_{T1}$ and $\mathbf{e}_{T2}$, are chosen based on their proximity to $\mathbf{e}_{Td}$. Then, both are alternately activated with different duty cycles, d_{T1}, and d_{T2}, so that the average torque can be aligned with $\mathbf{e}_{Td}$. The duty cycles are calculated to generate the desired tilting torque by taking a linear combination of both candidates as

$$d_{Td}\mathbf{e}_{Td} = d_{T1}\mathbf{e}_{T1} + d_{T2}\mathbf{e}_{T2} \tag{16}$$

where $$d_{T1} = d_{Td} \frac{(\mathbf{e}_{T1} \cdot \mathbf{e}_{T2})(\mathbf{e}_{Td} \cdot \mathbf{e}_{T2}) - (\mathbf{e}_{Td} \cdot \mathbf{e}_{T1})}{(\mathbf{e}_{T1} \cdot \mathbf{e}_{T2})^2 - 1} \tag{17a}$$

$$d_{T2} = d_{Td} \frac{(\mathbf{e}_{T1} \cdot \mathbf{e}_{T2})(\mathbf{e}_{Td} \cdot \mathbf{e}_{T1}) - (\mathbf{e}_{Td} \cdot \mathbf{e}_{T2})}{(\mathbf{e}_{T1} \cdot \mathbf{e}_{T2})^2 - 1} \tag{17b}$$

The magnitude of the tilting torque can be controlled by the desired tilting duty cycle d_{Td}.

TABLE I
SWITCHING TABLE

Switching index	Node 1	Node 2	Node 3	
1	0	+	−	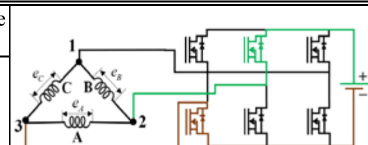
2	+	0	−	
3	+	−	0	
4	0	−	+	
5	−	0	+	Equivalent circuit of the driver
6	−	+	0	and stator poles for the switching index = 1

IV. Orientation Control

Fig. 2 illustrates the control structure for the SBLDC, implemented as a cascaded design consisting of three control loops: orientation control, angular rate control, and torque drive. This hierarchical approach allows for fine-tuning of performance specifications and offers flexibility in control mode selection. In this work, a P-PI control structure, commonly used for 3-dimensional orientation control of the quadrotor UAV [16], is employed. However, various controller can be applied to achieve specific control performance objectives, such as robustness and accuracy.

The orientation control computes the desired Euler angle rate using P control as

$$\dot{\boldsymbol{\eta}}_d = \mathbf{K}_{\mathrm{P,out}} \left(\boldsymbol{\eta}_d - \boldsymbol{\eta} \right) \tag{18}$$

where $\mathbf{\eta}_d = [\alpha_d, \beta_d, \gamma_d]^T$ is desired Euler angle, and P control gain $\mathbf{K}_{P,out}$ is a 3 by 3 diagonal matrix.

Angular rate control computes $\mathbf{T}_{\eta d}$, a desired generalized torque corresponding to the virtual displacement $d\mathbf{\eta}$. PI control can be applied for the angular rate control as

$$\mathbf{T}_{\eta d} = \mathbf{K}_{\mathrm{P,in}}\left(\dot{\mathbf{\eta}}_d - \dot{\mathbf{\eta}}\right) + \mathbf{K}_{\mathrm{I,in}}\int\left(\dot{\mathbf{\eta}}_d - \dot{\mathbf{\eta}}\right)dt \tag{19}$$

where $\mathbf{K}_{\mathrm{P,in}}$ and $\mathbf{K}_{\mathrm{I,in}}$ are 3 by 3 diagonal matrices

$\mathbf{T}_{\eta d}$ is converted to the desired torque expressed in the stator fixed frame, $\mathbf{T}_d = T_{Xd}\mathbf{e_X} + T_{Yd}\mathbf{e_Y} + T_{Zd}\mathbf{e_Z}$ as

$$\mathbf{T}_d = \mathbf{R}\mathbf{W}^{-T}\mathbf{T}_{\eta d} \tag{20}$$

$\mathbf{T}_d$ can be expressed by the desired duty cycles and directions of spinning and tilting torque as $\mathbf{T}_d = d_{Sd}\mathbf{e}_{Sd} + d_{Td}\mathbf{e}_{Td}$, where

$$d_{Sd} = \left|T_{Zd}\right|,\ d_{Td} = \left\|\begin{bmatrix}T_{Xd} & T_{Yd}\end{bmatrix}\right\| \tag{21}$$

$$\mathbf{e}_{Sd} = T_{Zd}d_{Sd}^{-1}\mathbf{e}_Z,\ \mathbf{e}_{Td} = d_{Td}^{-1}\left(T_{Xd}\mathbf{e}_X + T_{Yd}\mathbf{e}_Y\right) \tag{22}$$

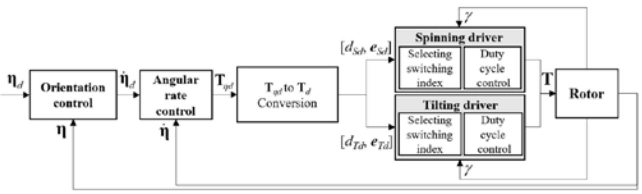

Fig. 2. Overall control structure.

V. Numerical Validation

A 6N8P SBLDC, detailed in Table II, is investigated to validate the proposed torque model and control system.

TABLE II
PARAMETERS OF THE 6N8P SBLDC

Rotor			
R_{PM} / t_{PM}	*32.5 / 3 mm*	a_{PM}	55°
PM remanence	1.35*T*	Maximum tilting angle λ_{max}	20°
Moment of inertia (I_a, I_b) / mass	(2.5e−5, 5e−5) $kg\cdot m^2$ / 0.1 kg	Drag coefficient *D*	−1e−3 *N·m·s*
Spinning layer		Tilting layers	
a / b / t	7.5 / 2.5 / 3 *mm*	*a / b / t*	5 / 2.5 / 3*mm*
Maximum current (for d_S =1)	5A	*Maximum current* (for d_T =1)	5A
Assembly of magnets	Stator EMs	Geometry of the EM	
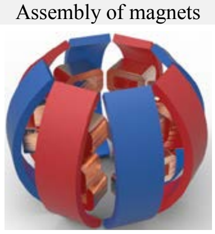	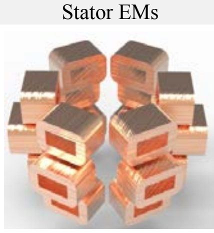	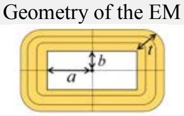 Geometry of the PM 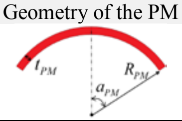	

A. Torque model and drive

The dominant magnetic fields are required to validate the torque model. They are extracted from the magnetic field in Fig. 3. The rotor and stator field are computed by a moment method based distributed multipoles (MMDMP). This method efficiently calculates magnetic fields and forces using a generalized magnetic source model [17]. The stator fields are computed for (d_S, d_T, k_S, k_T) = (1, 1, 1, 1) to obtain α_S and α_T. (11) and (13) are then computed and compared to the results from the MMDMP torque model in Fig. 4. Small differences are observed between the dominant harmonics torque model and the MMDMP, which can be attributed to the fact that the MMDMP can compute exact magnetic field of the PMs and EMs. Consequently, it considers interactions between all the rotor and stator field harmonics, while the proposed torque model only considers the dominant harmonics.

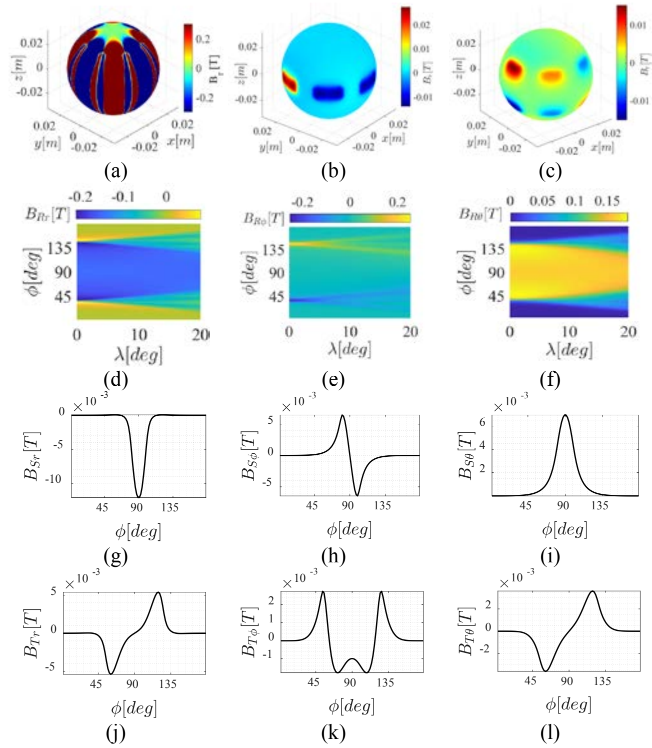

Fig. 3. Magnetic fields (a) Rotor field. (b) Spinning stator field. (c) Tilting stator field. (d) $B_{R r}$. (e) $B_{R\phi}$. (f) $B_{R\theta}$. (g) B_{Sr}. (h) $B_{S\phi}$. (i) $B_{S\theta}$. (j) B_{Tr}. (k) $B_{T\phi}$. (l) $B_{T\theta}$.

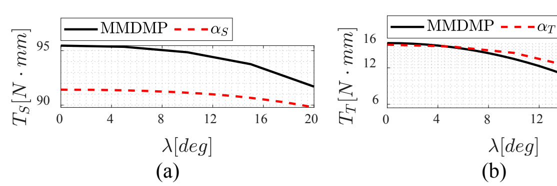

Fig. 4. α_S and α_T according to the tilting angle (a) α_S. (b) α_T.

The spinning torque in (10) is validated through a comparison with the results obtained from the MMDMP torque model. In Fig. 5(a), the spinning torque is investigated when the switching index is fixed at 1, and the rotor is tilted by 20°. The spinning torque changes with the spinning angle because of the variation in $\delta_{S\Delta}$. By altering the switching index to 2, the torque profiles are shifted by $\gamma = \pi/(3p_R)$ in Fig. 5(b) because δ_S shifts by $\pi/3$ as when the switching index k_S changes to 2. Hence, six torque candidates can be obtained based on δ_R, as shown in Fig. 5(c-d).

Similarly, tilting torque (12) is validated in Fig. 6. The torque model demonstrates good agreement with the MMDMP results in Fig. 6(a-b). In Fig. 6(c-d), the six torque candidates can be seen, and they rotate according to δ_R due to the change in $\delta_{T\Delta}$.

Fig. 7 depicts an example of the spinning torque drive. Fig. 7(a) displays the spinning torque driven with and without duty cycle control (15). Even without duty cycle control, the optimal torque candidate can be selected to maintain the torque direction. However, a torque ripple exists, as seen in the six-step commutation of a conventional BLDC. The use of duty control in Fig. 7(b) ensures consistent torque generation independent of the spinning angle.

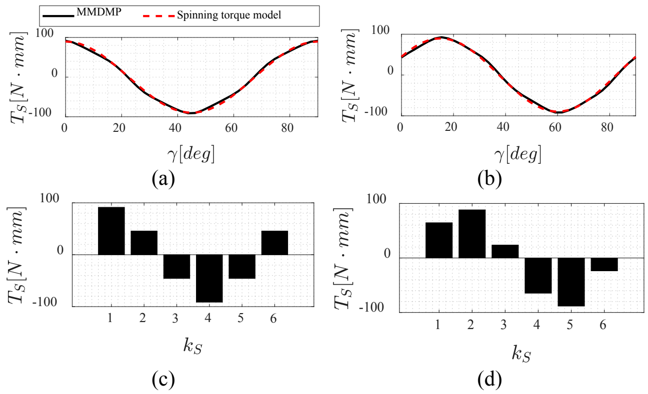

Fig. 5. Spinning torque model validation (a) (k_S, λ) = (1, 20°). (b) (k_S, λ) = (2, 20°). (c) T_S candidates for (δ_R, λ) = (0°, 0°) (d) T_S candidates for (δ_R, λ) = (45°, 0°).

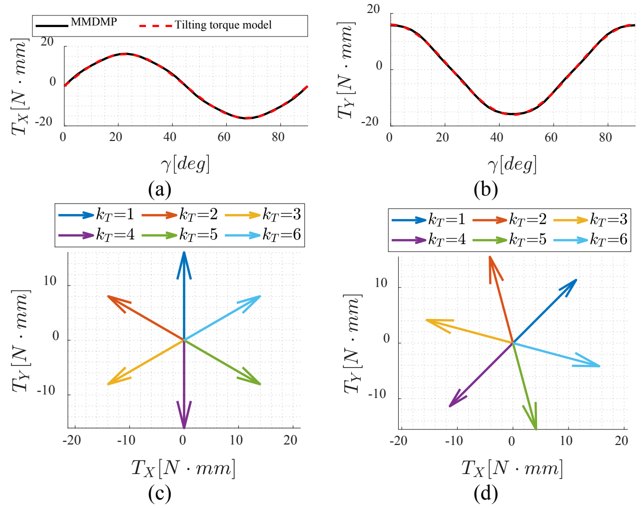

Fig. 6. Tilting torque model validation (a) T_X for (k_T, λ) = (1, 0°). (b) T_Y for (k_T, λ) = (1, 0°). (c) $\mathbf{T}_T$ candidates for (δ_R, λ) = (0°, 0°). (d) $\mathbf{T}_T$ candidates for (δ_R, λ) = (45°, 0°).

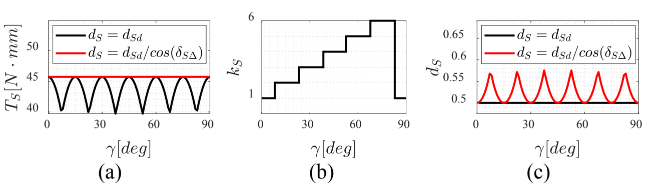

Fig. 7. Spinning torque drive (a) $\mathbf{T}_S$. (b) k_S. (c) d_S.

Fig. 8 illustrates the example of tilting torque drive along $\mathbf{e_X}$ where δ_R = 45°. As observed in Fig. 6(d), none of the torque candidates align with $\mathbf{e_X}$. Therefore, the closest torque candidates 1 and 6 are alternated with different duty cycles, as demonstrated in Fig. 8(c-d), with a switching frequency of 1kHz. By doing so, the average can be maintained in the direction along $\mathbf{e_X}$, as depicted in Fig. 8(a-b). The tilting torque can also be driven consistently, even with varying spinning angle δ_R = πsin(2πt), as shown in Fig. 9, where t is the simulation time.

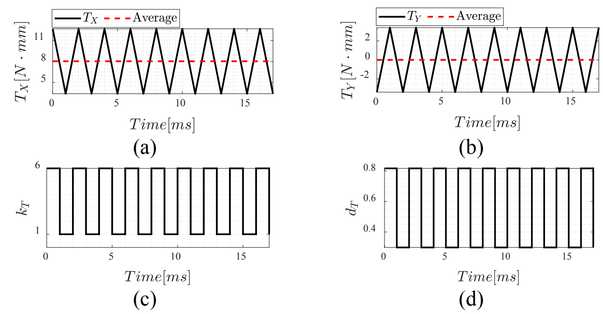

Fig. 8. Tilting torque drive for δ_R = 45° (a) T_X. (b) T_Y. (c) k_T. (d) d_T.

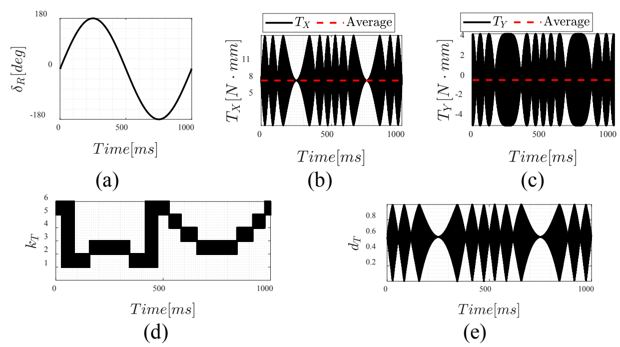

Fig. 9. Tilting torque drive for varying spinning angle (a) δ_R. (b) T_X. (c) T_Y. (d) k_T. (e) d_T.

B. Orientation control

The torque drive method is validated through its accuracy in orientation control. The gains for the orientation and angular rate control are set as $\mathbf{K}_{\mathbf{P,out}}$ = $diag$(200, 200, 100), $\mathbf{K}_{\mathbf{P,in}}$ = $diag$(0.1, 0.1, 0.1), and $\mathbf{K}_{\mathbf{I,in}}$ = $diag$(0.2, 0.2, 0.1), respectively. To ensure the average torque effect, the drive system is designed to operate at a much faster rate than the orientation controller. Therefore, the simulation loop for the driver is set at 1kHz, while the orientation control loop is set at 100Hz.

The step response of the control system is depicted in Fig. 10. The results show that the orientation of the system can quickly and accurately converge to the desired state, as seen in Fig. 10(a-c). The ability to quickly change the duty cycles and switching index, as shown in Fig. 10(e-h), also allows for the desired torque to be achieved.

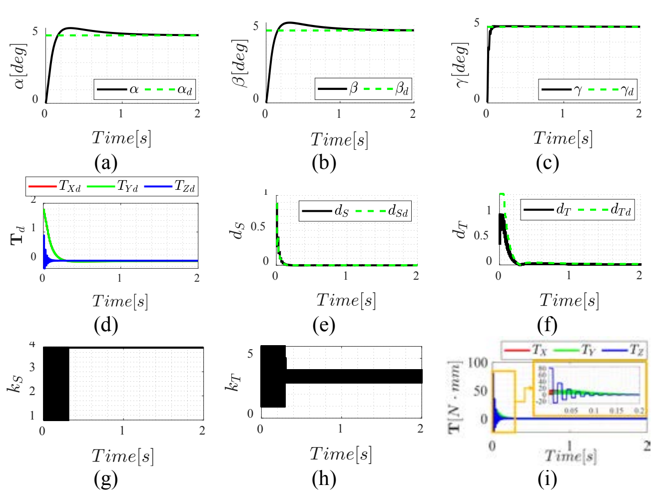

Fig. 10. Numerical simulation of the step response (a) α. (b) β. (c) γ. (d) $\mathbf{T}_d$. (e) d_S. (f) d_T. (g) k_S. (h) k_T. (i) $\mathbf{T}$.

The performance of the control system is further verified through the tracking simulation in Fig. 11, which demonstrates its ability to operate effectively even under varying spinning angles. This validation is essential because the spinning angle can significantly impact the phase difference between the rotor and the stator, affecting the torque output. Still, the proposed control system is designed to achieve desired torque generation, as seen in Fig. 11 (d) and (i).

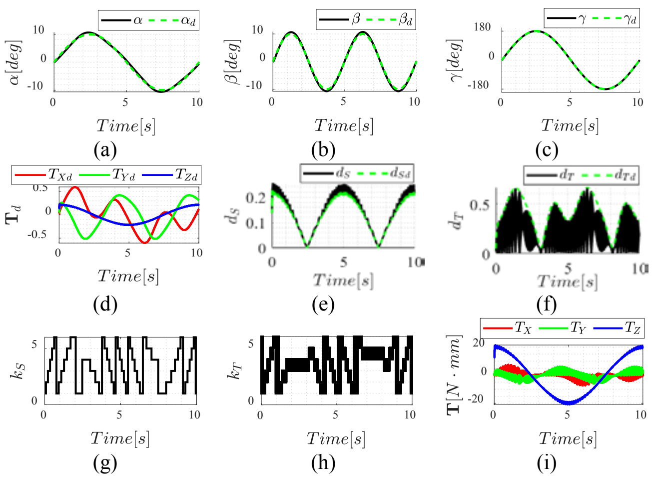

Fig. 11. Numerical simulation of the orientation tracking control (a) α. (b) β. (c) γ. (d) $\mathbf{T}_d$. (e) d_S. (f) d_T. (g) k_S. (h) k_T. (i) $\mathbf{T}$.

VI. Conclusion

In this paper, the SBLDC, a novel three-phase type spherical motor, was presented. The motor was designed based on conventional BLDC winding layouts and pole-slot combinations, and it featured separate spinning and tilting layers that could be controlled independently using two conventional BLDC drivers. The proposed torque drive method controlled both torque magnitudes and directions in three dimensions by manipulating the duty cycles of the drivers, which influenced the magnitude of the stator field. The method also involved selecting the proper switching index of the six-step commutation, which affected the phase of the stator field. One of the advantages of this drive method was that it did not require complex computation of the inverse torque model, making it simpler and more cost-effective. The effectiveness of the proposed torque drive method was validated through numerical simulations within a closed-loop controller. Future experimental validation will be conducted to demonstrate the potential of the SBLDC in the development of compact multi-DOF mechatronics systems.

Appendix A

Spinning Torque Model

The spinning torque acting on the rotor can be approximated as interaction between the dominant harmonics of the rotor (1) and the WH of the spinning layer (2). It can be derived based on the MST as

$$T_Z=\frac{-r_g^3}{\mu_0}\int_0^\pi s_\phi^2\int_{-\pi}^{\pi}B_rB_\theta d\theta d\phi= \tag{A.1}$$

$$\frac{-r_g^3}{\mu_0}\int_0^\pi s_\phi^2\int_{-\pi}^{\pi}\left(B_{Rr}c_{p_R\theta-\delta_R}+B_{Sr}s_{p_S\theta-\delta_S}\right)\left(B_{R\theta}s_{p_R\theta-\delta_R}+B_{S\theta}c_{p_S\theta-\delta_S}\right)d\theta d\phi$$

Due to the orthogonality of trigonometric functions, the spinning torque can be generated only for $p_S = p_R$. As a result, (A.1) can be simplified as

$$\begin{aligned}T_Z&=\frac{-r^3}{2\mu_0}\int_0^\pi s_\phi^2\int_{-\pi}^{\pi}\left(B_{S\theta}B_{Rr}+B_{Sr}B_{R\theta}\right)c_{\delta_{S\Delta}}d\theta d\phi\\&=-\pi\mu_0^{-1}r_g^3\int_0^\pi s_\phi^2\left(B_{S\theta}B_{Rr}+B_{Sr}B_{R\theta}\right)d\phi\cdot c_{\delta_{S\Delta}}\end{aligned}\tag{A.2}$$

References

[1] K.-M. Lee, H. Son, and J. Joni, “Concept development and design of a spherical wheel motor (SWM),” in Proc. IEEE ICRA, Barcelona, Spain, 2005, pp. 18–22.

[2] K. Bai, R. Xu, K.-M. Lee, W. Dai, and Y. Huang, “Design and development of a spherical motor for conformal printing of curved electronics,” IEEE Trans. Ind. Electron., vol. 65, no. 11, pp. 9190–9200, Nov. 2018.

[3] K. Bai, H. Yan, and K. M. Lee, “Robust control of a spherical motor in moving frame,” Mechatronics, vol. 75, May 2021.

[4] H. Son and K.-M. Lee, “Open-loop controller design and dynamic characteristics of a spherical wheel motor,” IEEE Trans. Ind. Electron., vol. 57, no. 10, pp. 3475–3482, Oct. 2010.

[5] H. Son and K.-M. Lee, “Control system design and input shape for orientation of spherical wheel motor,” Control Eng. Pract., vol. 24, pp. 120–128, Mar. 2014.

[6] H. Son and K.-M. Lee, “Two-DOF magnetic orientation sensor using distributed multipole models for spherical wheel motor,” Mechatronics, vol. 21, pp. 156–165, Feb. 2011.

[7] K. Bai and K.-M. Lee, “Direct field-feedback control of a ball-joint-like permanent-magnet spherical motor,” IEEE/ASME Trans. Mechatronics, vol. 19, no. 3, pp. 975–986, Jul. 2014.

[8] K. Bai, Y. Ding, Z. Que, H. Yan, X. Chen, S. Wen, and K.-M. Lee, "Regulation and Tracking Control of Omnidirectional Rotation for Spherical Motors," in IEEE Transactions on Industrial Electronics, vol. 70, no. 2, pp. 1696-1705, Feb. 2023.

[9] L. Gan, Y. Pei, and F. Chai, “Tilting torque calculation of a novel tiered type permanent magnet spherical motor,” IEEE Trans. Ind. Electron., vol. 67, no. 1, pp. 421–431, Jan. 2020.

[10] F. Chai, L. Gan, Y. Pei, and S. Cheng, "Tilting Torque Analysis of an Iron-Cored Tiered-Type Permanent Magnet Spherical Motor," IEEE Trans. Ind. Electron., vol. 68, no. 7, pp. 6121-6130, July 2021.

[11] F. Chai, L. Gan, and Y. Pei, "Torque Characteristic of a Novel Tiered Type Permanent Magnet Spherical Motor," IEEE Trans. Ind. Appl., vol. 56, no. 6, pp. 6338-6347, Nov.-Dec. 2020.

[12] F. Chai, L. Gan, and Y. Yu, “Magnetic field analysis of an iron-cored tiered type permanent magnet spherical motor using modified dynamic reluctance mesh method,” IEEE Trans. Ind. Electron., vol. 67, no. 8, pp. 6742–6751, Aug. 2020.

[13] F. Chai, L. Gan, and L. Chen, “A novel tiered type permanent magnet spherical motor and its rotor orientation measurement principle,” IEEE Access, vol. 8, pp. 15 303–15 312, 2020.

[14] S. Lee, “Spherical brushless direct current motor [SBLDC] - torque control,” *YouTube*, Aug. 1, 2022 [Video file]. Available: https://youtu.be/TXyc17zbCnA.

[15] Z. Q. Zhu, D. Ishak, D. Howe, and J. Chen, “Unbalanced magnetic forces in permanent-magnet brushless machines with diametrically asymmetric phase windings,” IEEE Trans. Ind Appl., vol. 43, no. 6, pp. 1544–1553, Nov./Dec. 2007.

[16] H. Lim, J. Park, D. Lee, and H. J. Kim, “Build your own quadrotor: Open-source projects on unmanned aerial vehicles,” IEEE Robot. Autom. Mag., vol. 19, no. 3, pp. 33–45, Sep. 2012.

[17] S. Lee, H. Kim, and H. Son, “Moment method based distributed multipoles for modeling magnetic materials in 2D and 3D magnetostatics,” Comput. Methods Appl. Mech. Eng., vol. 393, Apr. 2022.